



Recent Progress in Blue-Emitting Semiconductor Nanocrystal Quantum Dots for Display Applications

Seongwoo Cho^{1,2} · Yeongcheol Kim^{1,3} · Seunghyun Lee^{3,4} · Ju Young Woo^{1,3}

Received: 14 May 2024 / Revised: 16 July 2024 / Accepted: 22 July 2024

© The Author(s), under exclusive licence to Korean Institute of Chemical Engineers, Seoul, Korea 2024

Abstract

Solution-processable semiconductor nanocrystal quantum dots possess remarkable optical characteristics, including high photoluminescence quantum yield, narrow photoluminescence linewidth, and size-dependent color tunability. Three primary colors, which are red, green, and blue, are essential for realization of electroluminescent display utilizing quantum dots. While extensive research has been conducted on red- and green-emitting quantum dots, the development of blue-emitting quantum dots lags behind other primary color materials. This comprehensive review provides an overview of the progress in the synthesis of various types of blue-emitting quantum dots and their device applications. Furthermore, perspectives on further advancement of blue-emitting quantum dots to meet the requirements for commercially viable electroluminescent displays is discussed.

Keywords Blue-emitting quantum dot · Display · Electroluminescence · Commercialization

Introduction

Semiconductor nanocrystal quantum dots (QDs) have emerged as promising candidates for a variety of optoelectronic applications due to their unique size-dependent optical properties [1, 2]. Among the QDs with different colors, blue-emitting QDs hold particular significance in the development of next-generation displays, lighting, and biomedical imaging systems [3–7]. The realization of efficient and stable blue-emitting QDs with high color purity is crucial for achieving full-color displays and lighting with enhanced color reproducibility.

Despite significant progress in the synthesis and application of red- and green-emitting QDs, the development of blue-emitting counterparts has been more challenging. Blue emission typically requires larger bandgaps, which may pose challenges in synthesis and can lead to decreased photoluminescence (PL) quantum yield (QY) and stability. Furthermore, realizing blue-emitting color with PL peak around 460 nm, which is the most suitable for blue emission, and narrow emission linewidths both is very challenging [8, 9].

In recent years, however, there has been a surge at overcoming these challenges and advancing the field of blue-emitting QDs. This comprehensive review aims to provide an overview of the latest developments in the synthesis and application in various types of blue-emitting QDs. This review also provides insights into further developing blue-emitting QDs to make them suitable for commercial devices.

✉ Ju Young Woo
jywoo@kitech.re.kr

¹ Autonomous Manufacturing and Process R&D Department, Korea Institute of Industrial Technology (KITECH), Ansan 15588, Republic of Korea

² Department of Energy Science (DOES), Center for Artificial Atoms, Institute of Energy Science and Technology (SIEST), Sungkyunkwan University (SKKU), Suwon 16419, Republic of Korea

³ HYU-KITECH Joint Department, Hanyang University, Ansan 15588, Republic of Korea

⁴ Department of Chemical and Molecular Engineering, Hanyang University, Ansan 15588, Republic of Korea

Cd-Based QDs

Cd-based QDs such as CdS, CdSe, and CdS demonstrate their high PL QY and broad absorption spectra suitable for various optoelectronic devices. However, blue-emitting Cd-based QDs and device based on them exhibit very poor stability [10]. Many studies have been conducted to improve the quality of blue-emitting Cd-based QDs. This section aims

to provide an overview of the latest research trends in the synthesis and applications of blue-emitting Cd-based QDs.

Previously, research on the synthesis of Cd-based QDs encountered issues with size inhomogeneity. Slow and steady growth strategy was employed by using auxiliary substances such as TOP/TOPO solvent to enhance the size uniformity of various types of Cd chalcogenide QDs. This approach established the foundation for the progress of blue-emitting Cd-based QDs as shown in Fig. 1a [11]. Subsequently, the hot-injection approach was developed to improve spectral tunability of CdSe QDs in the blue spectral region by controlling the nucleation rate (Fig. 1b) [12]. It was found that surface passivations with inorganic (e.g., ZnS) or organic (e.g., alkylamine) shells are essential for enhancing PL QY of blue-emitting CdSe QDs. Similarly, the introduction of appropriate shell systems to CdS QDs enabled the suitable redshift of CdS-based QDs up to 460 nm, thus enabling their application in blue light emitting diodes (Fig. 1c) [13]. However, there has been an issue of lattice mismatch between Cd chalcogenides and Zn chalcogenides, which reduces the PL QY when the Zn chalcogenide shell system was introduced to Cd chalcogenide core QDs. To address this issue, cationic

alloy nanocrystals such as $Zn_xCd_{1-x}S$ and $Zn_xCd_{1-x}Se$ were developed by incorporating Zn into Cd chalcogenide QDs. The interfacial strain was mitigated due to reduced lattice mismatch between the core and shell, and therefore improved PL QY up to 55% was reported (Fig. 1d) [14]. The alloying strategy of anionic compositions was also developed under the presence of diphenyl phosphine to balance the reactivity of the anionic precursors. Higher emissivity and enhanced stability were observed in $CdSe_xS_{1-x}$ alloy QDs with gradient anionic compositions (Fig. 1e) [15].

In addition to the alloying strategy, employing multi-shell structures further helped enhance the performance of quantum dot light-emitting diodes (QLEDs) in the context of reducing lattice mismatch and aligning the energy levels for favorable charge transport, thereby enhancing the overall performance of optoelectronic devices. In the gradient shell systems like $CdSe_xS_{1-x}/ZnSe_yS_{1-y}$ with the emission range of 450–490 nm, interfacial lattice strain is effectively alleviated; therefore, high PL QY up to 90% and enhanced photochemical stability could be achieved (Fig. 2a) [16].

The development of giant shell QDs (g-QDs) with ultrathick shells was known to be very effective to obtain

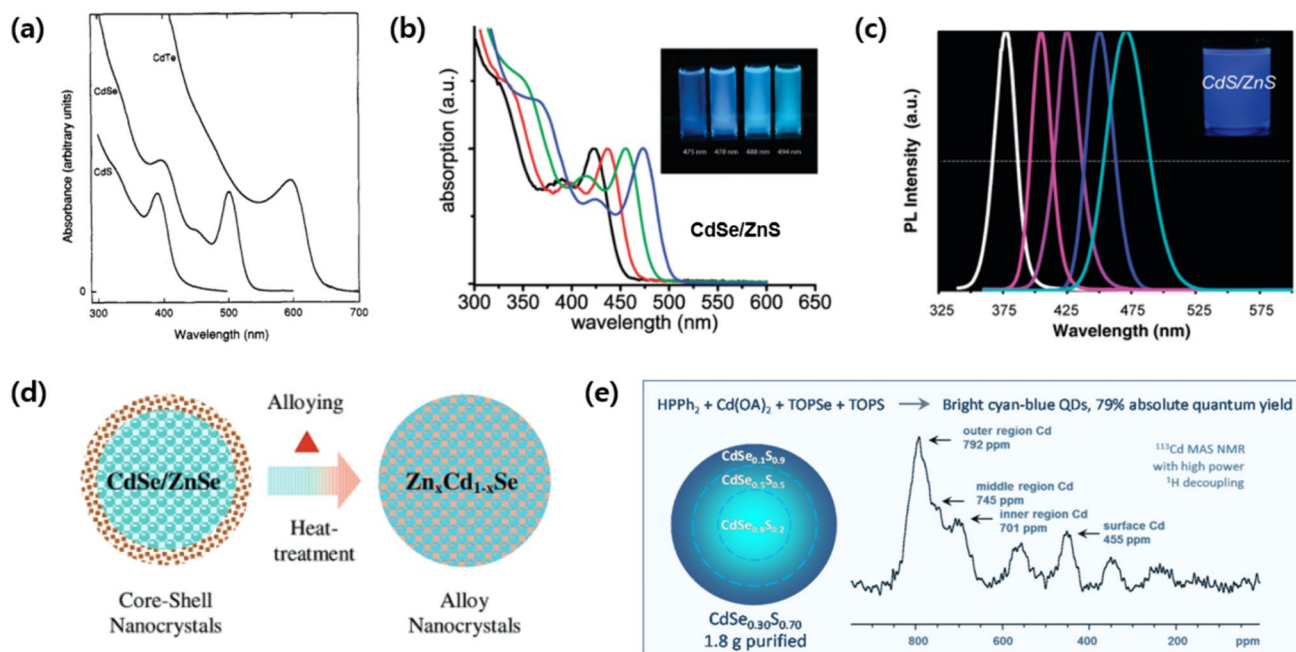


Fig. 1 **a** Absorption spectra of Cd chalcogenides with a diameter of ~2–3 nm. Adapted with permission from Ref. [11]. Copyright 1993 American Chemical Society. **b** Absorption spectra of CdSe/ZnS QDs depending on the time during synthesis. Adapted with permission from Ref. [12]. Copyright 2009 American Chemical Society. **c** PL spectra of CdS/ZnS QDs with different shell thickness. Adapted with permission from Ref. [13]. Copyright 2010 American Chemical Society. **d** A diagram depicting the kinetic alloying process transitioning from core-shell CdSe/ZnSe to alloyed $Zn_xCd_{1-x}Se$ nanocrystals.

Adapted with permission from Ref. [13]. Copyright 2003 American Chemical Society. **e** A schematic illustration of bright blue-emitting alloyed CdSeS QDs with a gradient structure, using HPPH₂ and solid-state NMR spectra of those QDs. The ¹¹³Cd magic angle spinning (MAS) spectrum, coupled with ¹H high-power decoupling (HPDEC), reveals the collective Cd signals situated at 701 ppm (inner core region), 745 ppm (middle region), and 792 ppm (outer region), marked by arrows in the bottom trace. Adapted with permission from Ref. [15]. Copyright 2016 American Chemical Society

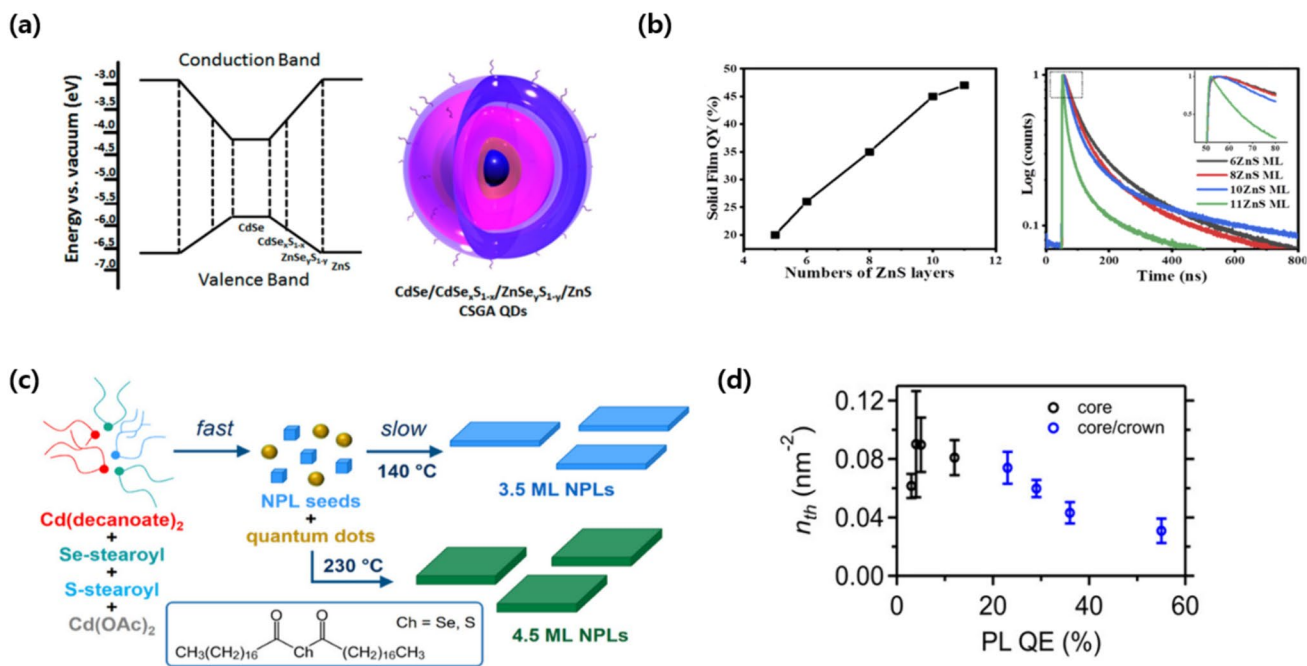


Fig. 2 **a** Energy band alignment of core/shell gradient alloy (CSGA) QDs (in eV) ranging from the CdSe core through the gradient alloy intermediate shells to the outer ZnS shells. Adapted with permission from Ref. [16]. Copyright 2017 American Chemical Society. **b** PL QY data (left) of compact QD films and temporal PL decay (right) for CdZnS/ZnS QDs with varying ZnS shell layers. Adapted with permission from Ref. [17]. Copyright 2020 Optica Publishing Group.

c Illustration of the synthetic procedure for CdSe_xS_{1-x} nanoplatelet. Adapted with permission from Ref. [18]. Copyright 2022 American Chemical Society. **d** The gain threshold of CdSe core and CdSe/CdS core/crown NPLs against PL QE. The error bars in the panels are derived from the gain threshold extraction procedure. Adapted with permission from Ref. [19]

high-quality QDs with strong chemical stability and high photostability. In addition, blinking behavior was significantly released in the blue-emitting g-QD system possibly due to suppressed interparticle interactions as illustrated in Fig. 2b [17].

The emergence of quasi 2-D structures such as nanoplatelets (NPLs) has led to rapid advancements for efficient blue emission. The synthesis of CdSe_xS_{1-x} NPLs allowed simple control of both compositions and thickness, enabling spectral extension from the blue to green regions. One of the expected challenging points in two anionic composition systems is difference in reactivity of the precursors. The reactivity difference of anionic precursors for the synthesis of CdSe_xS_{1-x} NPLs was mitigated by introducing stearoyl selenide and stearoyl sulfide as anionic precursors (Fig. 2c) [18]. In Cd chalcogenide-based NPL structures, photoluminescence quantum efficiency up to 55% was demonstrated by forming a CdS crown on the CdSe core. This represents a significant improvement compared to the 5–12% observed for core-only NPLs [19] (Fig. 2d).

With the remarkable advancements in Cd-based blue QDs as described above, the performance of blue QLEDs based on these materials has also been considerably improved. Currently, Cd-based blue-emitting QLEDs recorded EQE of 19.8%, a maximum luminance of 62,600 cd/m², and a T₅₀ greater than 10,000 h [20, 21].

Perovskite QDs

Perovskite QDs (PeQDs) typically consist of ABX₃ compositions where A and B are monovalent and divalent cations, respectively, and X is the halide anion. The PeQDs are also usually classified into organic–inorganic hybrid or all-inorganic perovskites depending on the A-site cations. While the bandgap of conventional QDs could be controlled by size tuning, the bandgap of PeQDs are usually controlled by manipulating the composition of halides. Despite the fact that the history of PeQDs is relatively short compared to that of conventional QDs, the EQE of green and red PeQD LEDs (PeQLEDs) has demonstrated remarkable advancements over 20% [22]. However, blue

PeQLEDs have shown much slower progress, achieving only 17.3% EQE to date [23]. This section will examine recent trends in the synthesis and application of blue-emitting PeQDs.

By adjusting halide compositions in mixed halide all-inorganic PeQDs, the PL spectra of deep blue (420–465 nm), pure blue (465–475 nm), and sky blue (475–495 nm) can be achieved. However, one of the drawbacks of blue-emitting all-inorganic PeQDs is a weak defect tolerance, and thus relatively lower PL QY compared with green- and red-emitting PeQDs. For example, in green- and red-emitting PeQDs based on Br and I halide compositions, the PeQDs are strongly tolerant against the halide vacancy defects; therefore, one can obtain relatively high PL QY even in the presence of such defects [24]. In contrast, it was known that blue-emitting PeQDs based on Cl halide composition are not strongly tolerant against halide vacancy defects presumably due to their wide band-gap. Hence, relatively lower PL QY has been reported in Cl-based blue-emitting PeQDs (Fig. 3a) [25].

Recently, Wang et al. performed various metal bromide salt (e.g., AgBr, PbBr₂, GeBr₂, ZnBr₂, CuBr₂, and InBr₃) treatment of CsPbCl₃ PeQDs to passivate the halide vacancy. The treatment resulted in significant enhancement of PL QY to near unity with spectral range at 450–470 nm.

Also, in LEDs fabricated based on PeQDs treated with metal halide salts, high phase stability under high applied bias was demonstrated (Fig. 3b) [26]. Cl vacancy suppresses radiative recombination and accelerates ion migration in the device, thereby impairing performance. Also Gao and his colleague introduced octylammonium hydrobromide ligands to enhance the efficiency and stability of perovskite blue LEDs by passivating the halide vacancy and thus to suppress ion migration in Cl/Br mixed PeQDs (Fig. 3c) [27]. In a similar context, Zheng et al. utilized a method to passivate Cl vacancy sites with pseudohalogens such as n-dodecylammonium thiocyanate and n-butylammonium thiocyanate. Treated PeQDs achieved a remarkable improvement with PL QY up to 100% at 468 nm of PL emission (Fig. 3d) [28].

Two-dimensional perovskite NPLs are also one of the promising candidates for blue-emitting perovskite materials to overcome phase segregation [29]. However, their colloidal stability can be poor possibly due to the weak surface ligand binding energy. In this case, introducing new capping ligands on the surface can provide better stability to CsPbBr₃ NPLs (Fig. 4a) [30]. For example, CsPbBr₃ NPLs with high surface-to-volume ratios are highly unstable. Additionally, organic ligands are easily detached from CsPbBr₃ NPLs, suppressing radiative recombination and deteriorating optical properties, along with poor conductivity within the film

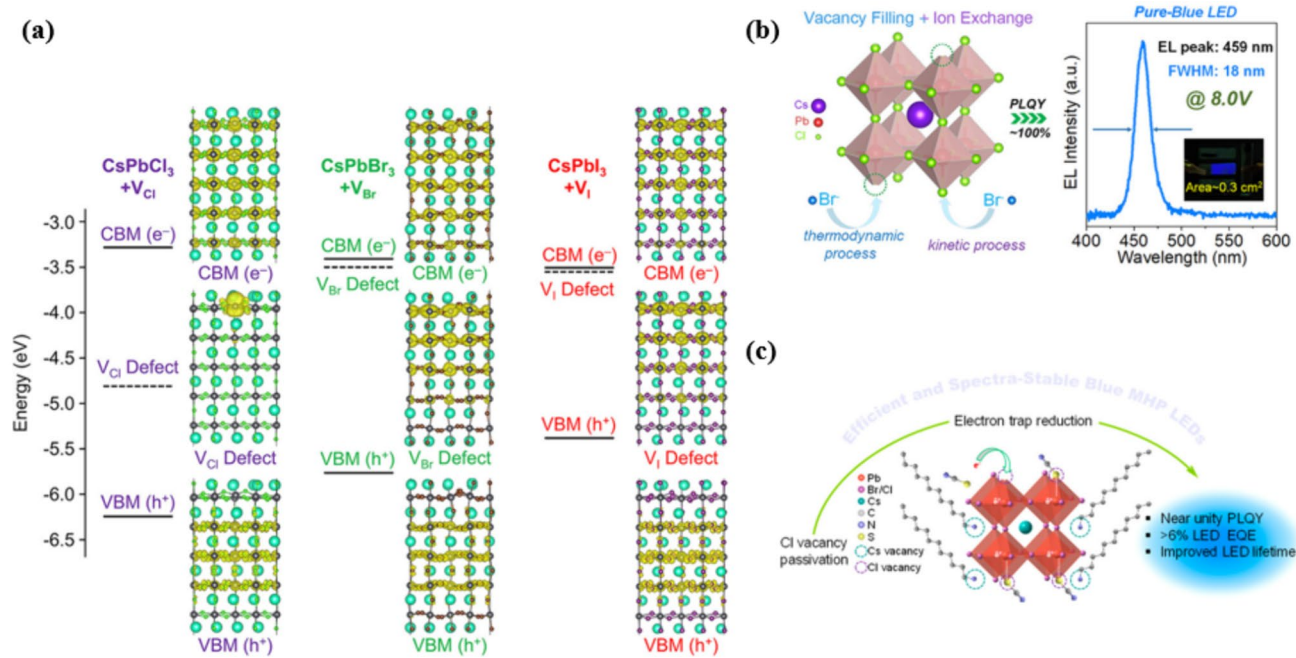


Fig. 3 **a** Electronic structure and charge density calculations according to halide vacancy (CsPbCl₃ + V_{Cl}, CsPbBr₃ + V_{Br}, CsPbI₃ + V_I). Adapted with permission from Ref. [25]. Copyright 2018 American Chemical Society. **b** Schematic illustrations of anion exchange reaction for vacancy passivation (left), normalized EL spectra (right). Adapted with permission from Ref. [26]. Copyright 2022 American

Chemical Society. **c** Illustration of the formation of Coulomb trap sites induced by Cl vacancies, electron trapping, and the self-assembly of organic thiocyanate on the defect sites in metal halide perovskites. Adapted with permission from Ref. [28]. Copyright 2020 American Chemical Society

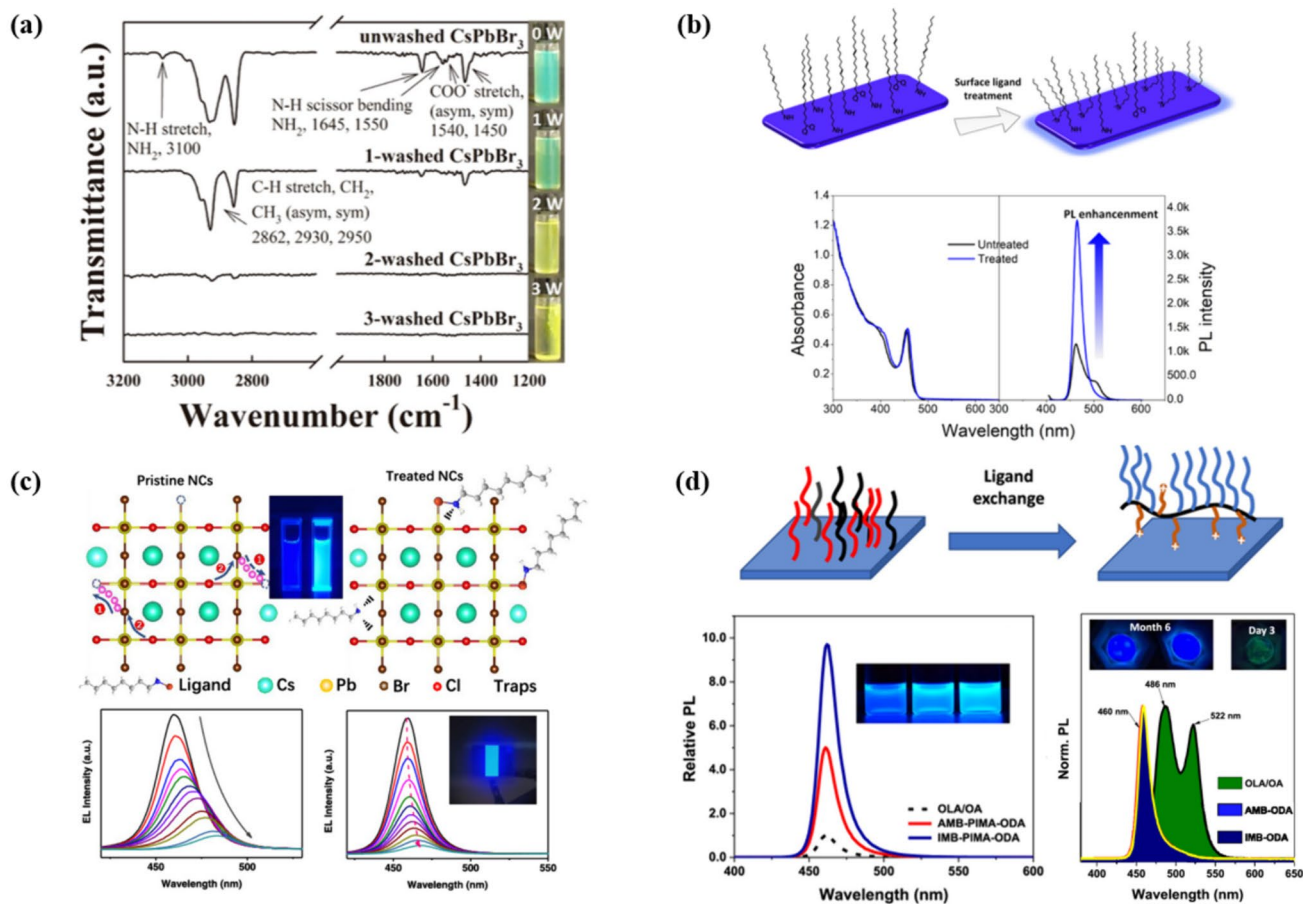


Fig. 4 **a** FTIR spectra and photos of CsPbBr₃ perovskites at various purification steps. Adapted with permission from Ref. [30]. Copyright 2015 American Chemical Society. **b** Schematic representation of the post-synthetic surface ligand treatment of CsPbBr₃ NPLs (top) Absorption and PL spectra (bottom). Adapted with permission from Ref. [32]. Copyright 2019 American Chemical Society. **c** Comparison of EL spectra from blue mixed-halide perovskite LEDs with and without octylammonium hydrobromide ligands. **d** Schematic illustrations of the interactions between the polysalt/PbBr₂ complex and the surfaces of NPLs (top). The relative photoluminescence meas-

ured for three different perovskite NPLs, reported in comparison to those of native oleic acid (OA)/oleylamine (OLA) or polysalt-coated materials. The inset photos: fluorescence images of those dispersions (bottom left). PL spectra collected from oleic acid (OA)/oleylamine (OLA)-coated nanocrystal perovskites (NPLs) aged in air for 3 days, and polysalt-coated NPLs aged in air for 6 months (bottom right). The photo of inset shows polysalt-coated NPLs (left) and OLA/OA-capped NPLs (right). Adapted with permission from Ref. [33]. Copyright 2022 American Chemical Society

[31]. Surface ligand engineering using di-dodecyldimethylammonium bromide contributed to preventing ligand detachment. This ligand system resulted in bright PeQDs with PL QY of 69.4% at 465 nm (Fig. 4b) [32].

Wang et al. reported the ligand exchange strategy of blue-emitting CsPbBr₃ NPLs with polysalt ligands produced by combining polymers and salt complexes. PL QY was eight times higher compared to untreated CsPbBr₃ NPLs. In the stability test, the CsPbBr₃ NPLs passivated with polysalt ligands exhibited high spectral stability without experiencing significant spectral shift for 6 months, while CsPbBr₃ NPLs with conventional OLA/OA ligand system showed considerable redshift only within 3 days (Fig. 4c) [33].

Zn-Based QDs

ZnSe QDs are very promising for blue-emitting applications due to their heavy metal-free compositions and a suitable bulk bandgap, which is around 2.7 eV, to achieve blue emission (Fig. 5a) [34]. At the early stage of the development of ZnSe QDs, the researchers usually employed synthesis based on aqueous phase, and the PL spectral range from 390 to 460 nm was achieved with the control of ZnS shell thickness. By fabricating a ZnSe/ZnS core/shell structure with thick ZnS shell, moderately improved PL QY of up to 45% was achieved (Fig. 5b) [35].

Further advancements have been made through developing the strategy separating nucleation and growth stages. Wang et al. successfully separated nucleation and growth

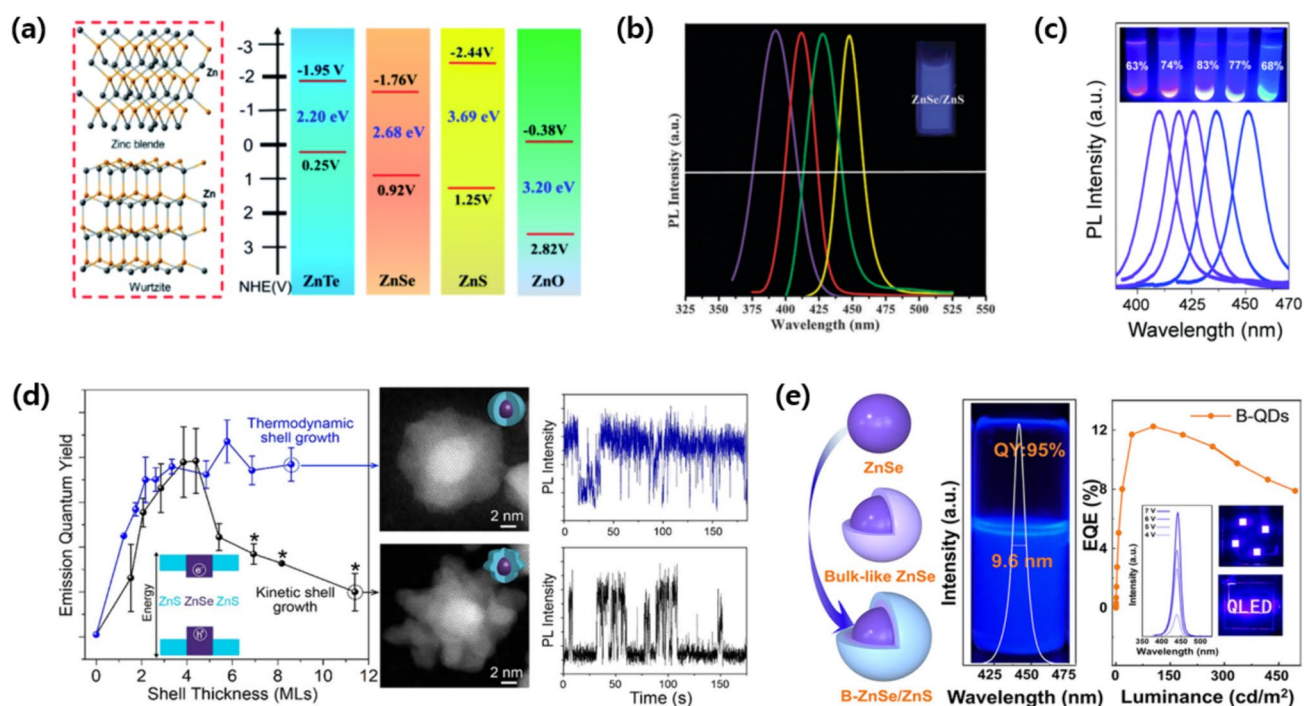


Fig. 5 **a** Crystal structures represented by zinc blende and wurtzite models of zinc chalcogenides. Adapted with permission from Ref. [34]. Copyright 2021 American Chemical Society. **b** PL spectra of zinc selenide/zinc sulfide core/shell QDs with varying core sizes, all of which were coated with 3.0 monolayers. Adapted with permission from Ref. [35]. Copyright The Royal Society of Chemistry 2010. **c** Normalized PL spectra of ZnSe/ZnS QDs, dispersed in hexanes, originated from ZnSe cores with adjustable PL peaks ranging from 400 to 455 nm ($\lambda_{\text{exc}} = 360$ nm). Adapted with permission from Ref. [36]. Copyright The Royal Society of Chemistry 2021. **d** The emission

quantum yield (QY), high-resolution STEM images, and representative time traces of the fluorescence intensity of ZnSe/ZnS core/shell QDs vary with the thickness of the shell. The molar ratio of Zn/oleic acid for the black color is 1/6.3, while for the blue color it is 1/10. Adapted with permission from Ref. [37]. Copyright 2020 American Chemical Society. **e** (from left to right) Synthetic scheme, PL spectrum, and EQE against luminance for the B(bulk)-like ZnSe/ZnS core/shell QDs (inset: EL spectra and QLED images of those QDs). Adapted with permission from Ref. [38]. Copyright 2020 American Chemical Society

stages by inducing each stage at low and high temperature, respectively, and finally yielding high-quality ZnSe/ZnS core/shell QDs with narrow PL spectra with FWHM of 20 nm and high PL QY over 80% (Fig. 5c) [36].

Furthermore, the researchers optimized the shell growth process with ZnS shell precursor with lower reactivity. As a result, FWHM and PL QY were further improved to 18 nm and 85%, respectively. The blinking also could be suppressed by controlling the morphology of the ZnS shell. After this morphology control of ZnS shell, improved on-time fraction of 75% was demonstrated (Fig. 5d) [37].

Du's group reported the synthesis of ZnSe-based QDs with giant ZnSe core. The size of the ZnSe core was increased by epitaxially growing ZnSe layers on ZnSe core, and finally 10.0 nm size of the ZnSe core was synthesized. The size is bigger than its exciton Bohr size. Extremely high PL QY was observed in ZnSe/ZnS QDs with a giant ZnSe core, and photostability was also improved. Furthermore, QLEDs fabricated with ZnSe/ZnS QDs with giant ZnSe core exhibited a maximum EQE of 12.2% and a relatively long operational lifetime ($T_{50} \sim 237$ h at 100 cd/m^2) (Fig. 5e) [38].

While the development of blue-emitting ZnSe-based QDs was very impressive, the ZnSe QDs have an inherent limitation to realize PL wavelength over 450 nm due to their bulk bandgap. In this context, ternary compound semiconductor ZnSeTe-based QDs were developed to extend the PL wavelength over 450 nm. The bandgap of ZnSeTe-based QDs can be tuned over broad spectral regions not only by changing their size, but also modifying the compositions of anionic species (Te/Se) (Fig. 6a and b) [39, 40]. By synthesizing heterostructure QDs based on multi-shells, PL QY over 80% was reported (Fig. 6c) [41]. Furthermore, by controlling the thickness of ZnSe midshell of heterostructure QDs, blue emission with very narrow FWHM could be realized (Fig. 6d) [42].

To successfully integrate blue-emitting ZnSeTe QDs in optoelectronic devices, their air stability should be improved. The PL QY of ZnSeTe-based QDs rapidly diminishes upon exposure, even if the QDs were formed in heterostructures with multi-shells. It is presumed that the degradation in blue-emitting ZnSeTe-based QDs can occur due to desorption of surface ligands in the presence

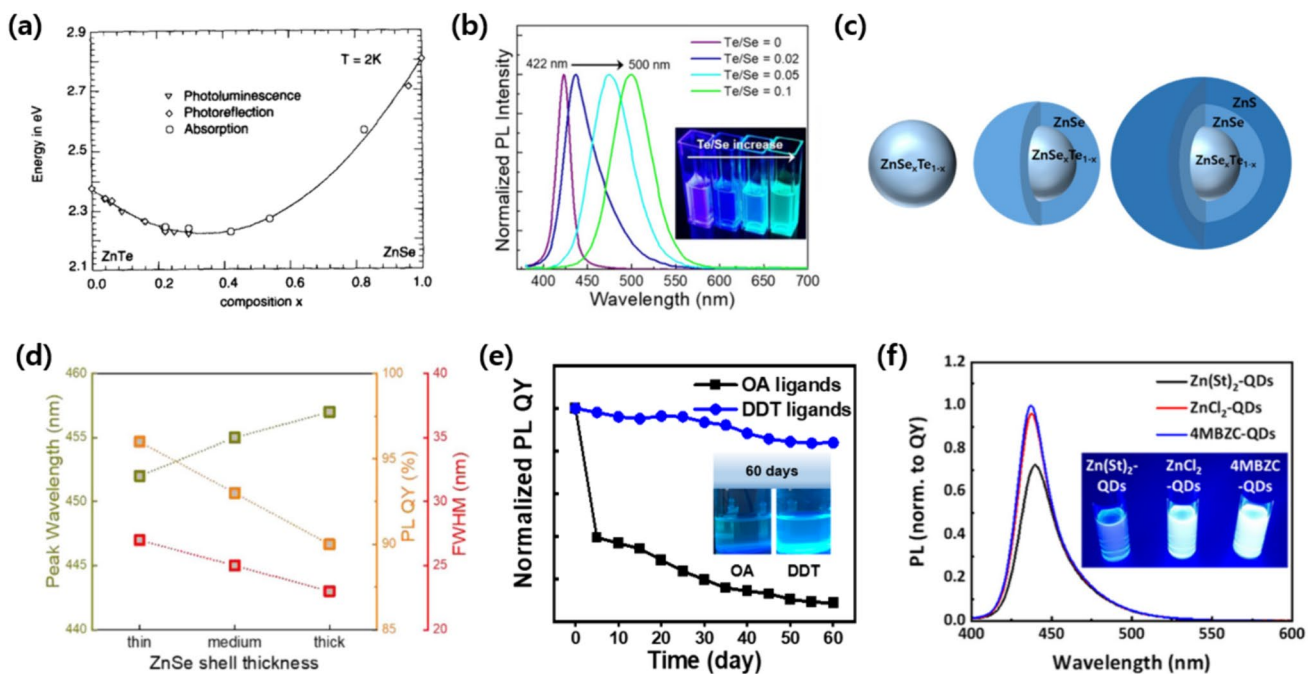


Fig. 6 **a** Experimental data of the bandgap energies for ZnSeTe materials. Adapted with permission from Ref. [39]. Copyright 1995 Published by Elsevier Ltd. **b** Normalized PL spectra of ZnSeTe/ZnS core/shell QDs varying with the Te/Se molar ratio. Adapted with permission from Ref. [40]. Copyright 2019 American Chemical Society. **c** Schematic illustration of ZnSeTe/ZnSe/ZnS multi-shell heterostructure system. Adapted with permission from Ref. [41]. Copyright 2020 The Korean Society of Industrial and Engineering Chemistry. Published by Elsevier B.V. All rights reserved. **d** Changes in the

peak wavelength, PL QY, and FWHM of ZnSeTe/ZnSe/ZnS QDs based on variations in the thickness of the ZnSe inner shell. Adapted with permission from Ref. [42]. Copyright 2021 Elsevier B.V. All rights reserved. **e** Stability data depending on surface ligand type of ZnSeTe/ZnSe/ZnS QDs (Oleic acid (OA), 1-Dodecanethiol (DDT)) Adapted with permission from Ref. [43]. Copyright 2022 American Chemical Society. **f** PL spectra and fluorescent images of Zn(St)₂-QDs, ZnCl₂-QDs, and 4MBZC-QDs are presented. Adapted with permission from Ref. [44]. Copyright 2023 American Chemical Society

of oxygen and moisture in the atmosphere. To mitigate this degradation, surface ligand exchange with stronger binding affinity can be a very effective strategy. Cho et al. reported that oleate-capped ZnSeTe/ZnSe/ZnS QDs can be considerably stabilized by exchanging their original carboxylate ligands to 1-dodecanethiol (DDT). The resulting ZnSeTe/ZnSe/ZnS QDs capped with DDT maintained 80% of their initial PL QY even after prolonged air exposure, and their photostability was also improved (Fig. 6e) [43].

Also, Lee et al. reported that the 4-methylbenzyl zinc chloride (4MBZC) ligand system effectively improved the stability of ZnSeTe-based QDs due to the dual passivation enabled by 4MBZC. As a result, PL QY over 84% of initial PL QY without any aggregation was demonstrated after air exposure of 1728 h (Fig. 6f) [44].

Even though the advancements in blue-emitting ZnSeTe-based QDs are impressive, light-emitting devices based on these QDs still suffer from serious instability. For example, the lifetime of blue-emitting QLEDs based on ZnSeTe-based QDs exhibits a very limited T₅₀ value of

15,850 h [45]. Furthermore, investigations of the degradation mechanisms of ZnSeTe-based QDs in devices have been nearly lacking. Future research should focus on a comprehensive understanding of the degradation mechanisms and developing strategies to enhance the stability, and therefore lifetime of QLEDs based on blue-emitting ZnSeTe QDs [46].

Other Blue-Emitting QDs with Heavy Metal-Free Compositions

InP-Based QDs

In recent studies, InP-based QDs have emerged as promising candidates for display materials, particularly in the green and red spectral regions, due to their suitable PL QY and color purity. Whereas the synthesis of InP-based QDs in pure and deep blue regions has been challenging for a long time, there are some recent insightful progress for the synthesis of InP QDs within the blue spectral regions [47].

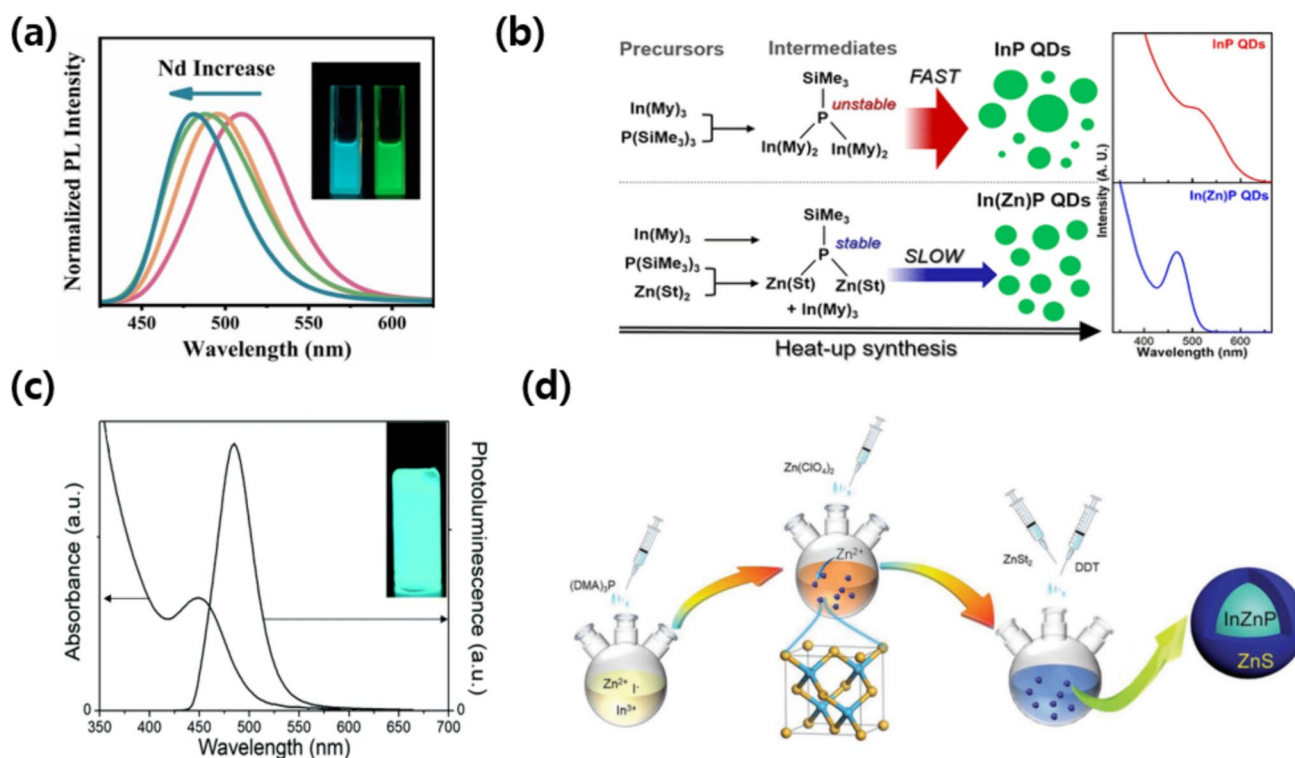


Fig. 7 **a** Normalized PL spectra of InP/ZnS QDs according to Nd amounts. Adapted with permission from Ref. [47]. Copyright 2022 John Wiley and Sons. **b** Schematic illustration of the effects of metal phosphorus of In(Zn)P QDs. Adapted with permission from Ref. [49]. Copyright 2017 American Chemical Society. **c** Absorption and

PL spectra of $\text{In}_{1-x}\text{Ga}_x\text{P}@ZnS$ QDs (picture of QDs under UV light (365 nm)). Adapted with permission from Ref. [50]. Copyright The Royal Society of Chemistry 2020. **d** Schematic illustration of the synthesis of In(Zn)P/ZnS QDs. Adapted with permission from Ref. [51]. Copyright 2023 John Wiley and Sons

Qin et al. introduced the rare earth neodymium (Nd^{3+}) ions at the interface of the InP core and ZnS shell for the first time, resulting in PL spectra around blue spectral regions with a narrow FWHM. The PL spectra of Nd^{3+} doped InP core QDs showed blue shift as the ratio of Nd^{3+} increased. The same trend was observed even with the ZnS shelling, resulting in the production of InP/ZnS QDs with emission center of 470 nm, FWHM of 46 nm, and PL QY of 44% (Fig. 7a) [48]. Lee and coworkers developed the synthesis of In(Zn)P QDs based on a heating-up method. Zn precursor was directly added during the synthesis of InP core QDs. It was known that Zn precursors forms Zn–P complexes by the reaction with a phosphine precursor molecule; therefore, the spectral linewidth of the resulting In(Zn)P-based QDs was narrow (Fig. 7b) [49]. The incorporation of Zn into InP is effective; however, forcing coordination of divalent cations can induce defect states within the bandgap. Gallium, which is the element from same group with indium, was employed to alleviate these defects states. The wider bulk bandgap of gallium compared to that of indium enables easier blue emission. The InGaP/ZnS blue QDs with gallium incorporation achieved PL QY of 65% (Fig. 7c) [50].

In a different context, improving the emission properties of InP-based QDs was investigated by properly choosing the additives. For example, it was recently reported that InP QDs synthesized under the presence of ZnI_2 showed better emission color purity compared to the InP QDs synthesized by adding ZnCl_2 . Addition of ZnI_2 to the synthesis of InP QDs resulted in smaller-sized QDs with the emission property at the blue spectral region. Furthermore, zinc perchlorate ($\text{Zn}(\text{ClO}_4)_2$) was introduced to further improve the size distribution and emission wavelength for blue color. Finally, InP/ZnS QDs with an emission peak wavelength of 466 nm, FWHM of 41 nm, and PL QY of 34% were produced (Fig. 7d) [51].

Carbon Dots

Recently, carbon dots (CDs) have garnered considerable attention due to their environmentally friendly nature, as well as their ability to adjust color, PL properties, size, shape, and doping. Also, due to such easily tunable properties, it had been considered that CDs can surpass other QDs based on conventional semiconductors. CDs were initially reported as fluorescent materials after properly purifying single-walled

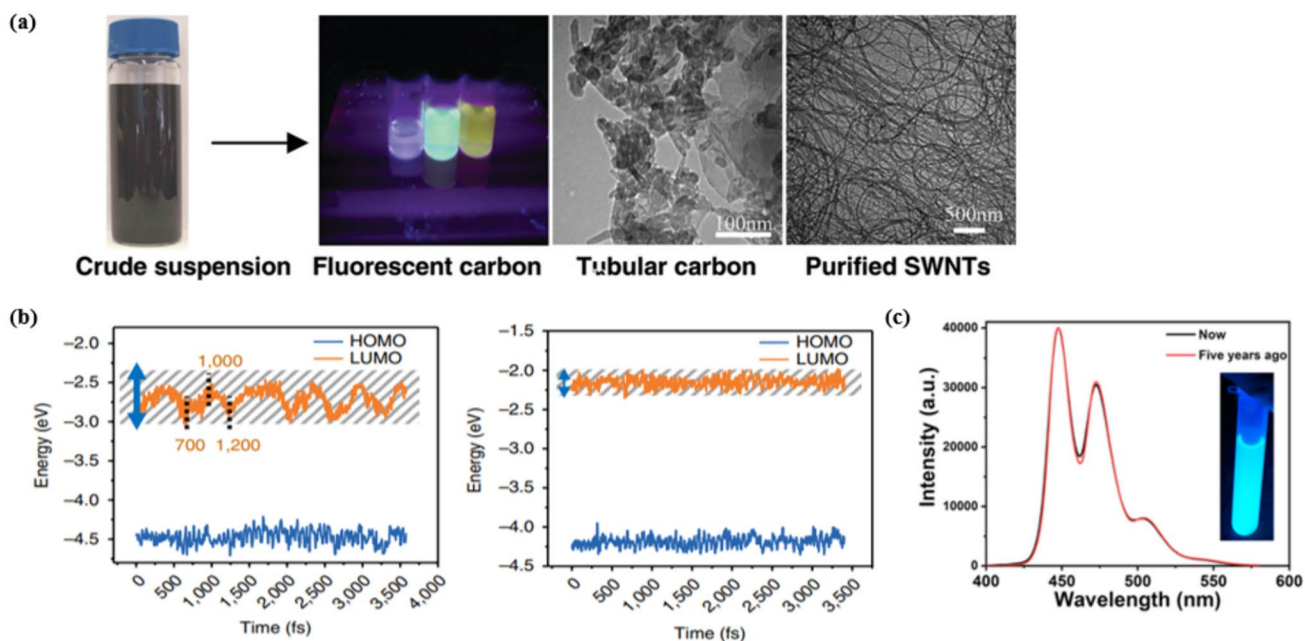


Fig. 8 **a** Image according to fractions of fluorescent carbon under UV lamp (365 nm) and TEM image. Adapted with permission from Ref. [52]. Copyright 2004 American Chemical Society. **b** The bandgap fluctuations of oxygen-containing functional groups (left) and

oxygen-free functional groups (right). Adapted with permission from Ref. [53]. Copyright 2020 Nature Publishing Group. **c** PL spectra of CDs (inset photo: CDs under UV lamp (365 nm)). Adapted with permission from Ref. [47]. Copyright 2021 John Wiley and Sons

carbon nanotubes using electrophoresis (Fig. 8a) [52]. Initial CDs showed very broad emission with an FWHM in PL spectrum over 80 nm. From the simulation study, it was confirmed that CDs functionalized with carboxylate group exhibit stronger polarization than CDs with amine functionality, finally leading to bandgap fluctuations and more delocalized wave functions and thus broad spectra (Fig. 8b) [53]. Amination of CDs enables efficient and high color purity emission by removing oxygen-containing functional groups. After amination, blue-emitting CDs with high PL QY of 70% with FWHM of 35 nm were synthesized.

Wang et al. reported the synthesis of CDs through the hydrothermal method with perylene-3,4,9,10-tetracarboxylic dianhydride (PTCDA) and 2,3-diaminophenazine (DAP). The resulting CDs were obtained as doped with oxygen and nitrogen, and exhibited strong and stable emission. The CDs showed very high PL QY of 88.9% with the emission center at 447 nm. LEDs fabricated based on the resulting CDs showed brightness of 648 cd m^{-2} and EQE of 2.114% (Fig. 8c) [54].

I–III–VI QDs

I–III–VI QDs, a promising candidate as an alternative to other QDs in the visible spectral region, have been previously studied in the green to red emission regions [55, 56]. While there was a challenge in synthesizing I–III–VI QDs

with emission wavelength in blue regions, Kim et al., for the first time, reported the synthesis of I–III–VI QDs with emission wavelength below 500 nm using CuGaS/ZnS QDs. The blue emission of CuGaS/ZnS QDs could be realized by adjusting the Cu/Ga ratio. Addition of Zn precursors during the core synthesis helped achieve further spectral blue shift. ZnS shelling also further induced spectral blue shift presumably due to enhanced quantum confinement, and the resulting QDs exhibited PL QY up to 83% at the blue spectral regions within 470–485 nm (Fig. 9a) [57].

To achieve wavelength in the deeper blue spectral region, AgGaS QDs can be utilized. By incorporating Zn precursors into AgGaS QDs, AgGaZnS QDs with deep blue emission can be synthesized. Additionally, by epitaxial shelling, ZnAgGaS/ZnS QDs can be formed with high PL QY of 58% at the deep blue spectral region around 450 nm (Fig. 9b) [58].

Achieving narrow FWHM in I–III–VI QDs is a challenging issue. Xie et al. reported relatively narrow FWHM in AgGaZnS-based QDs. The amount of Zn precursors was adjusted in the synthesis of AgGaZnS core QDs, and FWHM of 48 nm was demonstrated with PL QY of 16.7% in AgGaZnS-based QDs. By integrating AgGaZnS-based QDs into LEDs, a brightness of 123.1 cd m^{-2} a narrow of FWHM of 53 nm, and 0.4% of EQE were reported (Fig. 9c) [59].

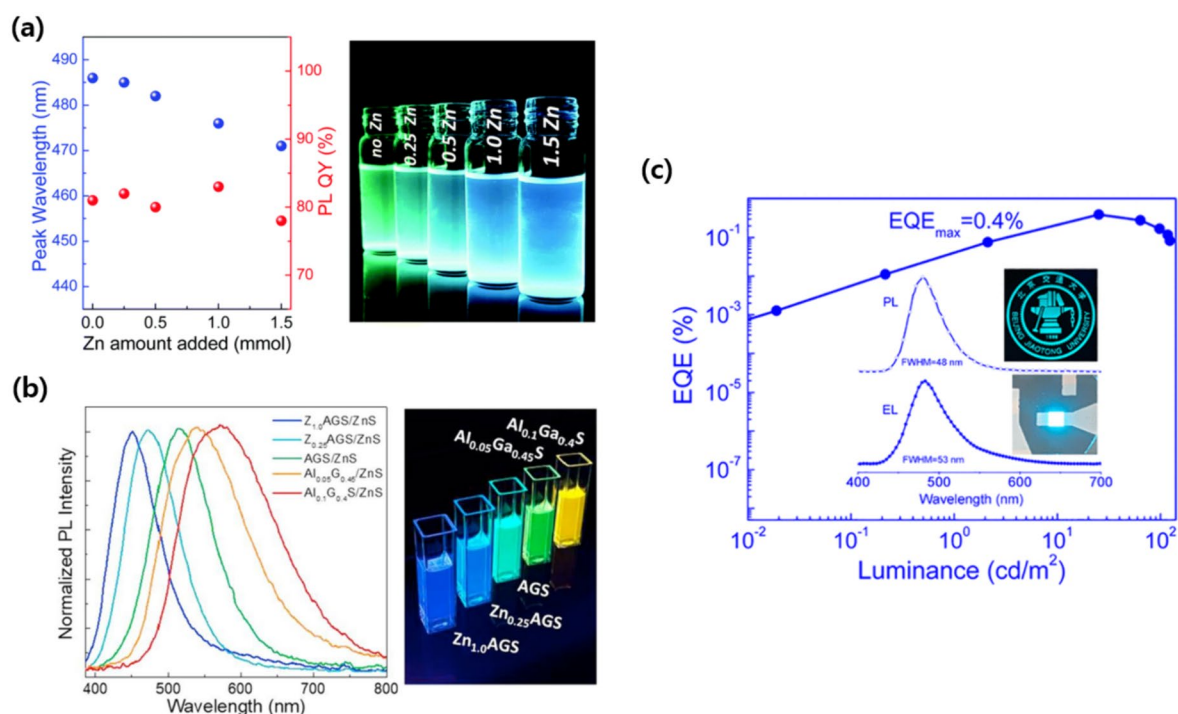


Fig. 9 **a** The peak wavelength and PL QY of ZnCuGaS@ZnS QDs according to the Zn precursor. Adapted with permission from Ref. [57]. Copyright The Royal Society of Chemistry 2017. **b** Normalized PL spectra of AgGaS@ZnS QDs according to Zn. Adapted with permission from Ref. [58]. Copyright 2018 Elsevier B.V. All rights

reserved. **c** EQE vs luminance curve of AgGaZnS QDs (inserted photo: PDMS film of dispersed AgGaZnS QDs UV excitation (top) emission of blue QLED (bottom)). Adapted with permission from Ref. [59]. Copyright 2022 American Chemical Society

Perspective and Conclusion

In summary, the remarkable progress in the development of blue-emitting QDs have brought them closer to being utilized in next-generation optoelectronics, particularly in display technology. Despite initial challenges, substantial advancement was achieved in synthesizing high-quality blue-emitting QDs with improved optical properties and stability. Nevertheless, to make higher-quality blue-emitting QDs which meet the standards of industry, color purity (emission linewidth) and stability (lifetime) should be further improved. In this context, we propose some research directions.

First, the research should be more focused on ZnSeTe-based QDs. Among various types of blue-emitting QDs, it is evident that ZnSeTe-based QDs are the most suitable candidates, up to date, considering their state of the art optical properties. By pushing further endeavors toward improving their optical properties, particularly emission linewidth and stability of electroluminescent devices based on them, we can step forward the realization of QD displays.

Secondly, it is imperative to conduct thorough research on alternative blue-emitting materials. Despite the fact that ZnSeTe-based QDs currently stand out as the leading

candidates for blue emission, there remains a possibility that their development for commercial electroluminescent display may not be entirely sufficient at the end. Therefore, the research on other alternative materials should be vigorously continued. Perovskite QDs can be a very strong alternative material. From industry, perovskite QDs received limited attention because most of the perovskite QDs contain heavy metal elements such as Pb. However, due to very outstanding optical properties of perovskite QDs, the attention from industry to perovskite QDs is rapidly increasing recently. If the perovskite QDs can meet the industrial criteria in optical properties and stability, with fulfilling RoHS regulation, commercialization of perovskite QDs could become reality. Additionally, as discussed in previous sections, carbon dots, I–III–VI QDs, and small-sized InP QDs with composition modifications also can be practical alternative materials for blue emission.

Finally, we note that the importance for developing of QDs is now increasing for realization of high-performance QD-based electroluminescent display. If researchers from both academia and industry consistently explore blue-emitting QD materials based on their efficient collaboration, we may be able to see widespread QD-based electroluminescent display in our lives.

Acknowledgements This work was supported by the Grants funded by the Ministry of Trade, Industry and Energy (00144108, 20015805, and 00423271) of the Korean government.

Declarations

Conflict of Interest The authors have declared that no competing interests exist.

References

- S. Neeleshwar, C.-L. Chen, C. Tsai, Y. Chen, C.C. Chen, S. Shyu, M. Seehra, *Phys. Rev. B* **71**, 201307 (2005)
- A. Litvin, I. Martynenko, F. Purcell-Milton, A. Baranov, A. Fedorov, Y. Gun'Ko, *J. Mater. Chem. A* **5**, 13252 (2017)
- T. Erdem, H.V. Demir, *Nanophotonics* **2**, 57 (2013)
- Q. Lin, L. Wang, Z. Li, H. Shen, L. Guo, Y. Kuang, L.S. Li, *ACS Photonics* **5**, 939 (2018)
- J. Kim, B. Koo, W.H. Kim, J. Choi, C. Choi, S.J. Lim, J.-S. Lee, D.-H. Kim, M.J. Ko, Y. Kim, *Nano Energy* **66**, 104130 (2019)
- S. Lim, J. Kim, J.Y. Park, J. Min, S. Yun, T. Park, Y. Kim, J. Choi, *A.C.S. Appl. Mater. Interfaces* **13**, 6119 (2021)
- T. Cheng, F. Wang, W. Sun, Z. Wang, J. Zhang, B. You, Y. Li, T. Hayat, A. Alsaed, Z. Tan, *Adv. Electron. Mater* **5**, 1800794 (2019)
- H. Qi, S. Wang, X. Jiang, Y. Fang, A. Wang, H. Shen, Z. Du, *J. Mater. Chem. C* **8**, 10160 (2020)
- J. Kim, J. Roh, M. Park, C. Lee, *Adv. Mater.* **36**, 2212220 (2024)
- L. Xi, J.Y. Lek, Y.N. Liang, C. Boothroyd, W. Zhou, Q. Yan, X. Hu, F.B.Y. Chiang, M.Y. Lam, *Nanotechnology* **22**, 275706 (2011)
- C. Murray, D.J. Norris, M.G. Bawendi, *J. Am. Chem. Soc.* **115**, 8706 (1993)
- R.K. Capek, K. Lambert, D. Dorfs, P.F. Smet, D. Poelman, A. Eychmüller, Z. Hens, *Chem. Mater.* **21**, 1743 (2009)
- D. Chen, F. Zhao, H. Qi, M. Rutherford, X. Peng, *Chem. Mater.* **22**, 1437 (2010)
- X. Zhong, M. Han, Z. Dong, T.J. White, W. Knoll, *J. Am. Chem. Soc.* **125**, 8589 (2003)
- J. Zhang, Q. Yang, H. Cao, C.I. Ratcliffe, D. Kingston, Q.Y. Chen, J. Ouyang, X. Wu, D.M. Leek, F.S. Riehle, *Chem. Mater.* **28**, 618 (2018)
- J. Cho, Y.K. Jung, J.-K. Lee, H.-S. Jung, *Langmuir* **33**, 3711 (2017)
- B. Xu, T. Zhang, X. Lin, H. Yang, X. Jin, Z. Huang, Z. Zhang, D. Li, Q. Li, *Opt. Mater. Express* **10**, 1232 (2020)
- A. Antanovich, L. Yang, S.C. Erwin, B. Martín-García, R. Hübner, C. Steinbach, D. Schwarz, N. Gaponik, V. Lesnyak, *Chem. Mater.* **34**, 10361 (2022)
- C. Rodà, A. Di Giacomo, L.C. Tasende Rodríguez, J. Leemans, Z. Hens, P. Geiregat, I. Moreels, *Nano Lett.* **23**, 3224 (2023)
- L. Wang, J. Lin, Y. Hu, X. Guo, Y. Lv, Z. Tang, Y. Fan, N. Zhang, Y. Wang, X. Liu, *ACS App. Mater. Interfaces* **9**, 38755 (2017)
- H. Shen, Q. Gao, Y. Zhang, Y. Lin, Q. Lin, Z. Li, L. Chen, Z. Zeng, X. Li, Y. Jia, S. Wang, Z. Du, L.S. Li, Z. Zhang, *Nat. Photonics* **13**, 192 (2019)
- K. Lin, J. Xing, L.N. Quan, F.P.G. de Arquer, X. Gong, J. Lu, L. Xie, W. Zhao, D. Zhang, C. Yan, *Nature* **562**, 245 (2018)
- S.Q. Sun, Y. Cai, M. Zhu, W. He, B.C. Liu, Y.L. Xu, X. Lv, Q. Sun, P. Liu, T. Shi, *Adv. Funct. Mater.* **33**, 2306549 (2023)
- L. Protesescu, S. Yakunin, M.I. Bodnarchuk, F. Krieg, R. Caputo, C.H. Hendon, R.X. Yang, A. Walsh, M.V. Kovalenko, *Nano Lett.* **15**, 3692 (2015)
- D.P. Nenon, K. Pressler, J. Kang, B.A. Koscher, J.H. Olshansky, W.T. Osowiecki, M.A. Koc, L.-W. Wang, A.P. Alivisatos, *J. Am. Chem. Soc.* **140**, 17760 (2018)
- X. Wang, T. Bai, X. Meng, S. Ji, R. Zhang, D. Zheng, B. Yang, J. Jiang, K.-L. Han, F. Liu, *ACS Appl. Mater. Interfaces* **14**, 46857 (2022)
- L. Gao, T. Cheng, L. Gou, Y. Zhang, Y. Liu, L. Yuan, X. Zhang, Y. Wang, F. Meng, J. Zhang, *ACS Appl. Mater. Interfaces* **15**, 18125 (2023)
- X. Zheng, S. Yuan, J. Liu, J. Yin, F. Yuan, W.-S. Shen, K. Yao, M. Wei, C. Zhou, K. Song, *ACS Energy Lett.* **5**, 793 (2020)
- H. Wang, F. Ye, J. Sun, Z. Wang, C. Zhang, J. Qian, X. Zhang, W.C.H. Choy, X.W. Sun, K. Wang, W. Zhao, *ACS Energy Lett.* **7**, 1137 (2022)
- Y. Wang, X. Li, S. Sreejith, F. Cao, Z. Wang, M.C. Stuparu, H. Zeng, H. Sun, *Adv. Mater.* **28**, 10637 (2016)
- Y. Kim, E. Yassitepe, O. Voznyy, R. Comin, G. Walters, X. Gong, P. Kanjanaboos, A.F. Nogueira, E.H. Sargent, *A.C.S. Appl. Mater. Interfaces* **7**, 25007 (2015)
- C. Zhang, Q. Wan, B. Wang, W. Zheng, M. Liu, Q. Zhang, L. Kong, L. Li, *J. Phys. Chem. C* **123**, 26161 (2019)
- S. Wang, W. Wang, S. Donmez, Y. Xin, H. Mattoussi, *Chem. Mater.* **34**, 4924 (2022)
- P. Li, T. He, *J. Mater. Chem. A* **9**, 23364 (2021)
- B. Dong, L. Cao, G. Su, W. Liu, *Chem. Commun.* **46**, 7331 (2010)
- A. Wang, H. Shen, S. Zang, Q. Lin, H. Wang, L. Qian, J. Niu, L.S. Li, *Nanoscale* **7**, 2951 (2015)
- B. Ji, S. Koley, I. Slobodkin, S. Remennik, U. Banin, *Nano Lett.* **20**, 2387 (2020)
- M. Gao, H. Yang, H. Shen, Z. Zeng, F. Fan, B. Tang, J. Min, Y. Zhang, Q. Hua, L.S. Li, B. Ji, Z. Du, *Nano Lett.* **21**, 7252 (2021)
- B. Freytag, P. Pavone, U. Rössler, K. Wolf, S. Lankes, G. Schötz, A. Naumov, S. Jilka, H. Stanzl, W. Gebhardt, *Solid State Commun.* **94**, 103 (1995)
- E.-P. Jang, C.-Y. Han, S.-W. Lim, J.-H. Jo, D.-Y. Jo, S.-H. Lee, S.-Y. Yoon, H. Yang, *A.C.S. Appl. Mater. Interfaces.* **49**, 46062 (2019)
- S. Park, C. Son, S. Kang, S. Baek, Y. Kim, O.-P. Kwon, J. Park, S.-W. Kim, *J. Ind. Eng. Chem. Ind. Eng. Chem.* **88**, 348 (2020)
- S.-H. Lee, S.-W. Song, S.-Y. Yoon, D.-Y. Jo, S.-K. Kim, H.-M. Kim, H.-M. Kim, Y. Kim, S.M. Park, H. Yang, *Chem. Eng. J.* **429**, 132464 (2022)
- S. Cho, S.N. Lim, H.S. Kim, S.A. Song, K. Kim, K.Y. Cho, J.Y. Woo, *A.C.S. Appl. Nano Mater.* **5**, 18905 (2022)
- B.J. Lee, T.Y. Kim, I. Kim, J.Y. Ryu, S. Jung, J.-U. Park, D.H. Yoon, Y. Choi, S.Y. Lee, T. Kim, *Chem. Mater.* **36**, 471 (2023)
- T. Kim, K.H. Kim, S. Kim, S.M. Choi, H. Jang, H.K. Seo, H. Lee, D.Y. Chung, E. Jang, *Nature* **586**, 385 (2020)
- O. Cho, S. Park, H. Chang, J. Kim, J. Kim, S. Kim, T. Kim and J. Kwak, *Nano Res.* **1**, 6527–6533 (2024)
- Z. Cui, D. Yang, S. Qin, Z. Wen, H. He, S. Mei, W. Zhang, G. Xing, C. Liang, R. Guo, *Adv. Opt. Mater.* **11**, 2202036 (2022)
- S. Qin, Z. Cui, Z. Wen, D. Yang, H. He, J. Zhao, M. Zhang, S. Mei, W. Zhang, R. Guo, *Appl. Surf. Sci.* **630**, 157483 (2023)
- S. Koh, T. Eom, W.D. Kim, K. Lee, D. Lee, Y.K. Lee, H. Kim, W.K. Bae, D.C. Lee, *Chem. Mater.* **29**, 6346 (2017)
- Y. Kim, K. Yang, S. Lee, *J. Mater. Chem. C* **8**, 7679 (2020)
- X. Zhou, J. Ren, W. Cao, A. Meijerink, Y. Wang, *Adv. Opt. Mater.* **11**, 2202128 (2023)
- X.Y. Xu, R. Ray, Y.L. Gu, H.J. Ploehn, L. Gearheart, K. Raker, W.A. Scrivens, *J. Am. Chem. Soc.* **126**, 12736 (2004)
- F. Yuan, Y.K. Wang, G. Sharma, Y. Dong, X. Zheng, P. Li, A. Johnston, G. Bappi, J.Z. Fan, H. Kung, B. Chen, M.I. Saidaminov, K. Singh, O. Voznyy, O.M. Bakr, Z.-H. Lu, E.H. Sargent, *Nat. Photonics* **14**, 171 (2019)

54. X. Wang, Y. Ma, Q. Wu, Z. Wang, Y. Tao, Y. Zhao, B. Wang, J. Cao, H. Wang, X. Gu, H. Huang, S. Li, X. Wang, F. Hu, M. Shao, L. Liao, T.K. Sham, Y. Liu, Z. Kang, *Laser Photon. Rev.* **15**, 2000412 (2021)
55. R. Sun, J. Zhao, O. Lin, Y. Li, X. Xie, W. Niu, Z. Yin, A. Tang, *J. Mater. Chem. C.* **12**, 4593 (2024)
56. S. Zhang, L. Yang, G. Liu, S. Zhang, Q. Shan, H. Zeng, A.C.S. *Appl. Mater. Interfaces* **15**, 50254 (2023)
57. B.Y. Kim, J.H. Kim, K.H. Lee, E.P. Jang, C.Y. Han, J.H. Jo, H.S. Jang, H. Yang, *Chem. Commun.* **53**, 4088 (2017)
58. J.H. Kim, B.Y. Kim, E.P. Jang, S.Y. Yoon, K.H. Kim, Y.R. Do, H. Yang, *Chem. Eng. J.* **347**, 791 (2018)
59. X. Xie, J. Zhao, O. Lin, Z. Yin, X. Li, Y. Zhang, A. Tang, *J. Phys. Chem. Lett.* **13**, 11857 (2022)

Publisher's Note Springer Nature remains neutral with regard to jurisdictional claims in published maps and institutional affiliations.

Springer Nature or its licensor (e.g. a society or other partner) holds exclusive rights to this article under a publishing agreement with the author(s) or other rightsholder(s); author self-archiving of the accepted manuscript version of this article is solely governed by the terms of such publishing agreement and applicable law.